Ultrafast generation and decay of a surface metal

L. Gierster[1*], S. Vempati[1,2], and J. Stähler[1,3]

[1]Fritz-Haber-Institut der Max-Planck-Gesellschaft, Abt. Physikalische Chemie, Faradayweg 4-6, 14195 Berlin, Germany
[2]Present address: Department of Physics, Indian Institute of Technology Bhilai, Raipur-492015, India
[3]Humbolt-Universität zu Berlin, Institut für Chemie, Brook-Taylor-Str. 2, 12489 Berlin, Germany
*corresponding author

Band bending (BB) at semiconductor surfaces or interfaces plays a pivotal role in technology, ranging from field effect transistors[1] to nanoscale devices for quantum technologies[2]. The control of BB via chemical doping or electric fields can create metallic surfaces with properties not found in the bulk, such as high electron mobility, magnetism or superconductivity[3,4]. Optical generation of metallic surfaces via BB on ultrafast timescales would facilitate a drastic manipulation of the conduction, magnetic and optical properties of semiconductors for novel high-speed electronics. Here, we demonstrate the ultrafast (20 fs) generation of a metal at the (10-10) surface of ZnO upon photoexcitation. This semiconductor is widely used in optoelectronics due to its transparency for visible light and its ease of nanostructuring[5,6]. Compared to hitherto known ultrafast photoinduced semiconductor-to-metal transitions (SMTs) that occur in the bulk of inorganic semiconductors[7], the SMT at the ZnO surface is launched by 3-4 orders of magnitude lower photon fluxes; also, the back-transition to the semiconducting state is at least one order of magnitude faster than in previous studies of other materials[8]. Using time- and angle-resolved photoelectron spectroscopy, we show that the SMT is caused by photoinduced downward surface BB due to photodepletion of deep surface defects. The resulting positive surface charges pull the conduction band below the equilibrium Fermi level, similar to chemical doping. The discovered mechanism is not material-specific and presents a general route for controlling metallicity confined to semiconductor interfaces on ultrafast timescales.

When the doping density of shallow donors is increased above a critical value in a semiconductor, the excess electrons, originally localized in hydrogenic potentials at impurity sites, delocalize and form a metallic band[9]. Remarkably, this Mott or Mott-Anderson transition happens already at low doping densities, for example at parts per 10^4 atoms in phosphorous-doped silicon[9]. SMTs also occur in two-dimensions at semiconductor surfaces leading to the formation of two-dimensional electron gases (2DEGs)[10]. In the case of oxide surfaces, this is often caused by surface doping with shallow donor defects such as oxygen vacancies[11,12] or adsorbates as, for instance, hydrogen[13,14]. The positively charged impurity sites modify the surface potential, causing downward BB of the conduction and valence band (CB and VB, respectively) towards the surface. As the CB bends below the equilibrium Fermi level E_F, it becomes partially filled and a 2DEG forms.

Beyond chemical doping, metal-like properties of semiconductors can also be generated by optical excitation. At low photoexcitation densities the optical and electronic response of semiconductors is dominated by non-interacting free carriers and excitons. In contrast, strong photoexcitation can lead to metal-like behavior by three different mechanisms:

1. At a critical excitation fluence the so-called exciton Mott transition occurs, above which an electron-hole plasma forms with quasi-Fermi levels in the CB and VB[15,16]. In this case, the material may exhibit metal-like optical properties and conductivities; however, as there is no density of states around the equilibrium Fermi level E_F, no true SMT has occurred.
2. A real SMT can be achieved by photoinduced changes to the electronic band structure for instance due to strong carrier-lattice or carrier-carrier interactions that change the screening of the Coulomb interaction[7,17,18]. Yet, in the case of inorganic semiconductors, strong laser excitation (mJ/cm^2) is necessary to drive such photoinduced phase transition (PIPT), as in the famous room temperature PIPT in vanadium dioxide[19–22]. Due to the high energy uptake, the SMT usually becomes thermally stabilized, and the recovery of the equilibrium phase is limited by thermal dissipation processes of nanosecond duration[8].
3. Analogous to chemical doping, the band structure can also be optically manipulated by photodoping[23–25]. One photodoping mechanism is the photoexcitation of deep donors, which creates electron-hole pairs bound in hydrogenic potentials, exhibiting properties similar to the shallow donors discussed above[26]. When their density is enhanced, metallicity can be achieved[27]. This transition can be metastable and lead to persistent photoconductivity, as observed in various semiconductors[27,28]. Amongst them is the wide band gap (3.4 eV), intrinsically n-doped (E_F ca. 0.2 eV below the CB) semiconductor ZnO, which has a variety of native deep donor defects leading to a broad photoluminescence signal below the fundamental band gap energy[29,30]. However, an ultrafast PIPT due to photodoping by depopulation of deep donor defects has not yet been demonstrated neither in the bulk nor at the surface of a semiconductor.

In this article, we unveil an ultrafast photoinduced SMT confined to the surface of ZnO using extremely low excitation fluences with sub-ns decay and feasible up to at least 256 K. This dramatic effect is enabled by photodoping of the surface: depopulation of deeply bound in-gap (defect) states induces transient downward surface BB. Above a threshold fluence of only 13.6 μJ/cm^2, the photoexcited electrons delocalize in a non-equilibrium state that shows all defining footprints of a metal: Density of states around the equilibrium Fermi energy E_F resulting from a partially filled dispersive band and an electron distribution following Fermi-Dirac statistics that thermalizes with the lattice within 200 fs. We track the PIPT in the time domain by monitoring the photodoped electron density, the nearly-free electron mass of the surface electrons, and the energy shift of the VB. Generation and decay of the

surface metal occur on the timescales of electronic screening and electron-hole recombination, respectively. The carrier density of the surface metal shows the same build-up and decay dynamics as the downward shift of the VB that occurs upon positive charging of the surface by photoexcitation. Remarkably, this is the first demonstration of a photoinduced SMT confined to the surface of a semiconductor and the mechanism does not require photoinduced changes to the band structure beyond surface BB; a sufficiently large number of deep donor levels should enable similar effects at the surfaces of many n-doped semiconductors.

To probe the PIPT, we use time- and angle-resolved photoemission spectroscopy (trARPES) and a ZnO sample of (10-10) orientation cleaned in ultrahigh vacuum (cf. Methods). We excite the sample resonantly with the band gap ($h\nu_{pump}$ = 3.43 eV) and use time-delayed (Δt) probe pulses with $h\nu_{probe}$ = 6.3 eV, photoemitting electrons from the transiently occupied CB (energy level diagram in Fig. 1a). Fig. 1b shows the photoemission (PE) intensity, which is proportional to the density of occupied electronic states, versus Δt and energy with respect to E_F for a pump laser fluence above the threshold for the SMT. The sample exhibits a large photoresponse below the equilibrium E_F, which persists for several hundred ps. A video of the angle-resolved spectra as a function of Δt gives an impression of the process (available as supplemental material). The angular distribution of the pump-induced change, averaged from 4-8 ps, is shown in Fig. 1c. It exhibits a broad feature of few 100 meV width, which is cut by E_F and shows a curvature, to the eye most apparent at low energies. We can extract the curvature by fitting the data with a Gaussian peak multiplied by a Fermi-Dirac distribution (other methods give the same result, see Extended Data Fig. 1). The peak positions describe a parabola with m_{eff} = 1.2(1) m_e, i.e. the band exhibits nearly the free electron mass m_e. Thus, after photoexcitation, ZnO shows the characteristic of a metal: a dispersive band, cut by the equilibrium E_F, indicative of a SMT.

To further confirm the above finding we analyze the angle-integrated PE spectra in the first ps after excitation (Fig. 1d). The excitation of metals with fs laser pulses initially leads to a heating of the electronic subsystem and a subsequent equilibration with the phonon bath within the first ps[31]. Photoexcited ZnO behaves analogously to photoexcited metals: The spectra exhibit a characteristic change of the high energy tail around E_F which can be described by a Fermi-Dirac distribution with a delay-dependent temperature (data and fits in Fig. 1d, cf. Methods). The resulting time-dependent electronic temperature is plotted in the inset of Fig. 1d. Starting at 1300 K, it decays due to equilibration with the lattice within approx. 200 fs. The photoinduced phase thus shows electron-electron and electron-phonon interaction as expected for a metal.

To quantify the temporal evolution of the PIPT, we spectrally integrate the photoinduced electron signal below E_F (purple), which is proportional to the electron density in the metallic band, and plot its time dependence together with the evolution of the band curvature $1/m_{eff}$ (green markers) in Fig. 2a.

Electron density and curvature of the metallic band show a two-fold build-up (τ_1 = 20(20) fs, τ_2 = 1.20(15) ps), which is followed by a decay on a timescale of hundreds of ps (τ_3 = 219(13) ps); see Methods for details on the fitting. The effective mass is a measure of the electron localization in real space[32,33]. The rise of $1/m_{eff}$ can be viewed as dynamic delocalization of the photoexcited electrons and the subsequent decrease of $1/m_{eff}$ during the decay as dynamic localization[33]. The degree of localization is correlated with the photoexcited electron density. We conclude that the free electron-like metal is generated abruptly within the experimental resolution on the time scale of electronic screening[16,34] and decays on a sub-nanosecond timescale.

In order to determine the PIPT threshold fluence we tune the excitation fluence across a wide range, from few to tens of $\mu J/cm^2$. Fig. 2b shows the curvature $1/m_{eff}$ as a function of fluence. Below the threshold fluence of F_c = 13.6 $\mu J/cm^2$, the pump laser pulse induces an electron population below E_F with a flat angular distribution (Extended Data Fig. 2), indicative of a localized electronic state[32] as expected for an exciton[34]. Moreover, no hot electron gas cooling is observed. Thus, low fluence photoexcitation creates a localized, non-interacting electron population. Above F_c, $1/m_{eff}$ increases monotonously and, simultaneously, the hot electron gas cooling starts developing (Extended Data Fig. 2); we find $m_{eff} = 0.7\ m_e$ for the highest fluence in our experiment. This confirms the connection of the degree of localization and the carrier density observed in the time dependence. The PIPT threshold F_C corresponds to an excitation density of 2.7 10^{24} m^{-3}, which agrees well with literature values of the Mott density (1-3 10^{24} m^{-3}) in ZnO[35,36]. While, above F_C, a transient surface metal is generated, the excited carriers do not interact beyond exciton formation in the low fluence regime, consistent with earlier work on weakly photoexcited ZnO surfaces[37].

We showed that a photoinduced SMT occurs in ZnO. The transient metal phase has the properties of an equilibrium metal: the quasi-E_F in the CB equals the equilibrium E_F for all excitation densities (cf. Fig. 1c and extended data Fig. 2). Therefore, the SMT goes beyond a pure exciton Mott transition: a photoinduced change of the electronic band structure must occur to shift the CB from its equilibrium position 200 meV above E_F down to below E_F (cf. the sketch in Fig. 1a). The band structure could be changed via band gap renormalization (BGR) due to carrier-carrier screening[15]. BGR would shift the CB downward, and at the same time the VB would move upward[38]. On the contrary, for the photodoping mechanism introduced above the VB should shift downward: Depopulation of deep donor levels creates positive surface charges which lead to downward BB.

In order to distinguish the BGR and the photodoping scenario, we determine the energetic position of the VB upon photoexcitation. A probe photon energy of $h\nu_{probe}$= 4.25 eV gives access to the VB in a two-photon photoemission process. Fig. 3b compares a VB spectrum at negative delays (black) to one at a positive pump-probe delay of few ps (red). Clearly, the VB is transiently shifted to lower energies. The false color plot in Fig. 3a shows that the downward shift occurs abruptly and persists for several

hundred ps. Based on this, we exclude BGR as the driving mechanism and conclude that surface BB caused by photodoping is the origin of the PIPT. Note that the VB shift is not entirely rigid but that the peak also appears broadened and has a lower amplitude (Fig. 3b). This observation is consistent with surface BB, where not all probed unit cells along the surface normal exhibit the same shift, as noted previously for chemical doping[11].

Beyond monitoring band positions, trARPES offers another direct way of probing that the surface is indeed positively charged after photoexcitation: As shown previously for GaAs[39], a change of the surface charge leads to a short-range electrostatic field in the near-surface vacuum region that affects photoelectrons that just escaped the sample. Consequently, in a pump-probe experiment, photoelectrons emitted by the probe would be decelerated by a pump-induced positive surface charge at small negative pump-probe delays $\Delta t < 0$, when the photoelectrons are still close to the surface[39]. Clearly, the data in Fig. 1b shows such downward shift of the surface electron signal probed by $h\nu_{probe} = 6.3$ eV for $\Delta t < 0$ on a 100 ps timescale. This unambiguously demonstrates that the surface is positively charged due to photoexcitation by the pump laser pulse. Note that such photoinduced changes of the surface charge and the resulting change of surface BB are well-known as surface photovoltage phenomena[40]. Both, increase and decrease of BB have been demonstrated in the ultrafast time domain[41].

The final link between downward BB and the SMT is given in Fig. 2a, where we compare the VB shift as a function of Δt (black markers) to the time-dependent electron density in the metallic band (XC, purple markers) obtained under the same excitation conditions. As evidenced by a global fit (blue curve), both transients agree perfectly for all time scales, from ultrafast (abrupt and delayed) rise to decay. We conclude that photoinduced downward surface BB drives the SMT, as illustrated in the sketch in Fig. 3c.

Photoexcitation will charge the surface positively and lead to the SMT only if the pump photon energy is sufficient to excite electrons from deep donor levels to normally unoccupied states. By tuning the pump photon energy below the fundamental gap of 3.4 eV[30] we can exclusively address in-gap states. As before, the energetic position of the VB in the time domain unveils whether the surface is charged positively by photoexcitation. Fig. 3d,e show that downward BB is induced upon photoexcitation with $h\nu_{pump} = 3.2$ eV (full width half maximum: 0.1 eV) but not with $h\nu_{pump} = 3.0$ eV. Thus, the deep donor levels responsible for the SMT lie closer than 0.4 eV above the VB maximum. Such deep in-gap states can be caused by lattice vacancies[30], which are created at the surface upon annealing in ultra-high vacuum[42].

In Fig. 4, we illustrate the photodoping mechanism and the associated time scales of the photoinduced processes. The pump laser pulse depopulates deep donor defects at the surface and populates the CB with electrons (process 1). Subsequently, with $\tau_1 = 20(20)$ fs, downward surface BB occurs. The CB

bends below E_F and is partially filled. Simultaneously, the CB electrons delocalize, generating the surface metal phase. This delocalization occurs above a critical electron density only, in analogy to the Mott-Anderson transition driven by chemical doping with shallow donors. After the abrupt laser excitation, the downward BB, the electron density of the surface metal, and the degree of delocalization increase further with τ_2 = 1.20(15) ps. We interpret this as hole trapping at surface defect sites (process 2), which charges the surface even more positively and leads to an increase in surface BB. A resolution-limited upper boundary of 80 ps for this process was recently identified by X-ray absorption spectroscopy[43] and few-ps time constants were determined by optical spectroscopy[29]. However, we note that hole polaron formation[44] may result in similar dynamics. Eventually, the CB electrons recombine with the surface defects and, as the doping density is reduced, the electrons localize (increasing m_{eff}) with τ_3 = 219(13) ps (process 3). This back-transition to the semiconducting state is at least one order of magnitude faster than, for example, the decay of the photoinduced SMT in VO_2[8]. It should be noted that a fraction of the photodoped and localized surface electrons show lifetimes exceeding the inverse repetition rate of our laser system (5 μs), consistent with defect exciton lifetimes extending to the μs regime[29]. Interestingly, the above processes do not require cryogenic temperatures: The PIPT can be realized between 100 K up to at least 256 K, i.e. close to room temperature (Extended Data Fig. 3).

In summary, we unveiled a photoinduced ultrafast SMT at the surface of ZnO with an extraordinarily low threshold fluence. The mechanism is simple and universal: Photodepletion of in-gap states (deep defects) causes photodoping of the surface, which leads to downwards BB of the CB below E_F. All our experimental observations are consistent with this mechanism, from positive surface charging and downward BB that occurs simultaneous with the SMT, to the (dynamic) delocalization of the surface electrons. The same mechanism should lead to PIPTs at surfaces or interfaces of other semiconductors with a sufficiently high density of deep surface defects. Beyond technological implementations of ZnO as an ultrafast, transparent photoswitch with the transient properties of an equilibrium metal, this work is the starting point for studies of 2DEGs with emerging properties beyond metallicity in the ultrafast time domain.

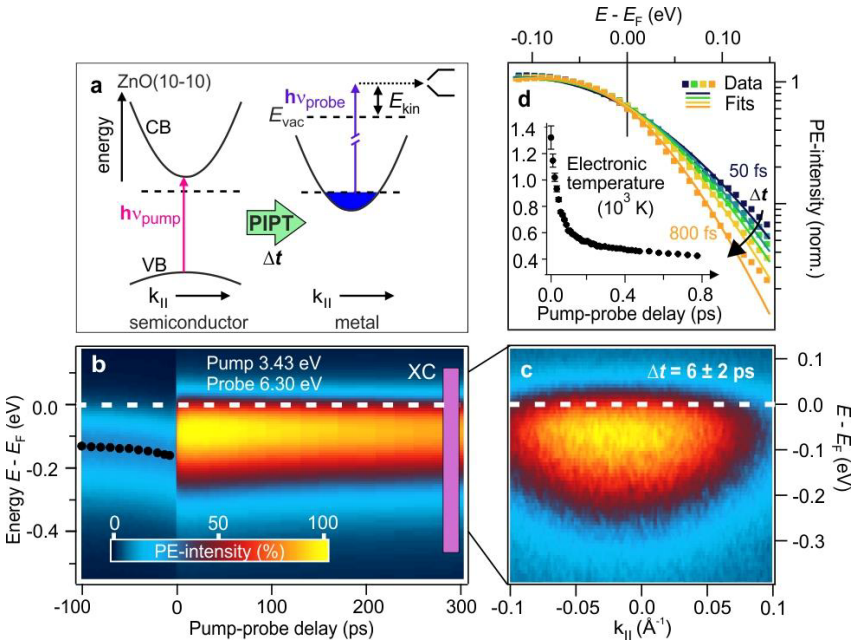

Figure 1 Time-resolved photoelectron spectroscopy of the ZnO(10-10) surface upon resonant excitation. a, Energy level diagram and illustration of the discussed photoinduced phase transition. b, PE-intensity in false colors as a function of pump-probe delay Δt and energy. Probe: 6.3 eV, pump: 3.43 eV (27 μJ/cm²). The pump pulse induces an abrupt increase of the electron density below E_F. The purple box (XC) indicates the energy-integration window for the evaluation shown in Fig. 2. c, Angle-resolved PE-intensity averaged from 4 to 8 ps showing a dispersive free electron-like band. d, Normalized, angle-integrated PE-intensity for different delays (50 to 800 fs) with Fermi-Dirac distribution fits (solid lines). Inset: Electronic temperature versus Δt.

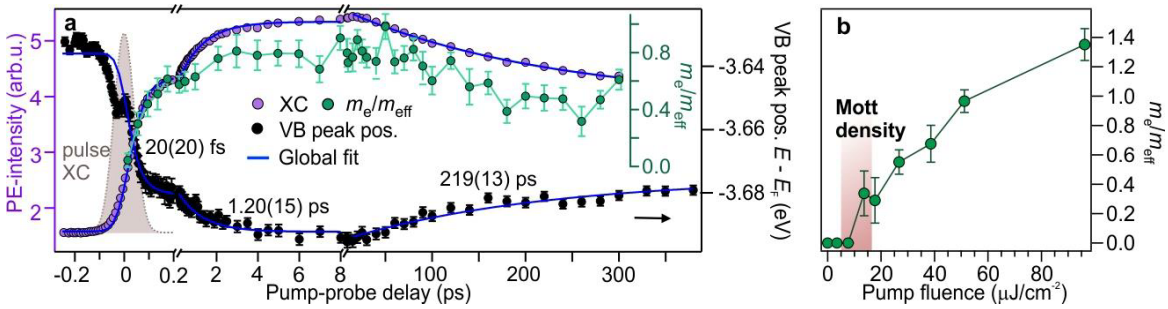

Figure 2 Dynamics and fluence dependence of surface metallization. a, Purple: PE-intensity below E_F (proportional to the surface electron density). The energy-integration window is indicated by the purple box (XC) in Fig. 1a. Green: Curvature of the metallic band (determination see Extended Data Fig. 1). Black: VB peak position (determination see Fig. 3). The blue line is a global fit (see Methods). Grey area: Instrument response function. b, Fluence-dependent evolution of the band curvature. Error bars respresent standard deviations.

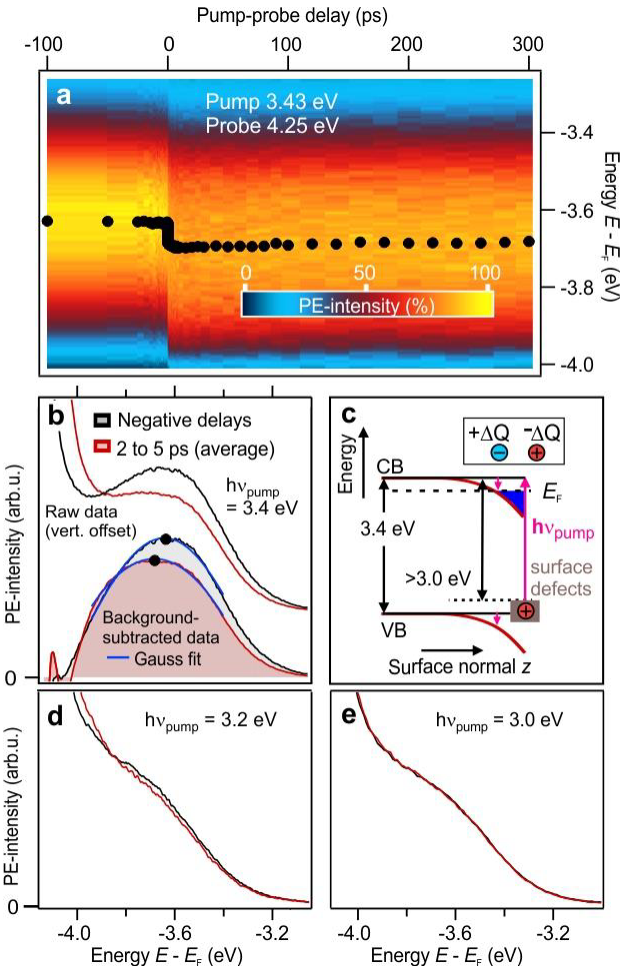

Figure 3 Downward shift of the VB upon resonant and below band gap excitation. a, PE-intensity from the VB in false colors as a function of pump-probe delay probed by two-photon photoemission with $h\nu_{probe}$ = 4.25 eV. Pump: 3.43 eV (27 μJ/cm²). Markers: peak positions, determination see b. b, Comparison of VB spectra at negative delays (black) and at positive delays (red). Top: Raw data (vertically offset for clarity). Bottom: Data after subtracting the background of secondary electrons. Blue: Gaussian fits to determine the peak maximum. c, Energy level diagram with a sketch of downward surface BB along the surface normal z. d, e VB spectra at negative (black) and positive delays (red) for different pump photon energies below the fundamental gap.

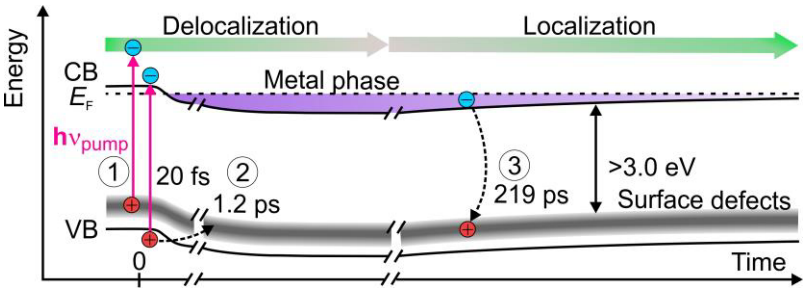

Figure 4 Scheme of the pump-induced processes. Resonant pumping populates the CB and depopulates surface defect states leading to downward surface BB; the electrons delocalize and form the metal phase (process 1). Delayed increase of the BB occurs due to hole trapping at surface defect sites (process 2). The PIPT recovers as the surface charge is reduced by electron-hole recombination (process 3).

Methods

The ZnO(10-10) sample was purchased from MaTeck GmbH and is prepared by repeated cycles of Ar^+-sputtering (0.75 keV, 8 μA) succeeded by 30 min annealing in ultra-high vacuum (T_{max} = 950 K, heating rate 30-40 K min^{-1}). The surface cleanliness is confirmed by LEED and photoemission measurements of the work function. The VB maximum lies at -3.2 eV with respect to E_F (Fig. 3b). The E_F reference is taken from the gold sample holder, which is in electrical contact with the sample surface.

Photoemission measurements are performed in situ using a hemispherical electron energy analyzer (PHOISBOS 100, Specs GmbH). A bias voltage of 1.5 eV is applied with respect to the sample. Pump and probe laser pulses are generated from a regenerative amplifier system running at 200 kHz and several optical parametric amplifiers (OPAs) working at 200 kHz (PHAROS, internal OPA, Orpheus-2H, Orpheus-3H by Light Conversion). 6.3 eV laser pulses are reached by frequency quadrupling of the 1.55 eV output of the internal NOPA. Pump pulses with 3.2-3.4 eV and probe pulses with 4.25 eV are created in the Orpheus-2H and 3H, respectively. All measurements shown in the main text are performed at 100 K.

The fit functions for extracting the time constants (Fig. 2a) consists of a double exponential rise and a single exponential decay convolved with a Gaussian peak representing the cross correlation of pump and probe laser pulses. The latter is determined from high energy cuts in the ZnO pump-probe data in case of using 6.3 eV as probe photon energy, yielding a cross correlation width of 115(17) fs (full width half maximum). In the case of using 4.25 eV as probe photon energy, the cross correlation is measured in situ by pump-probe photoemission from a tantalum sheet yielding 71(1) fs (full width half maximum). The rise and decay time constants are the result of a global fit to the PE intensity around E_F and to the VB shift, as shown in Fig. 2a. The time resolution in the experiments is limited by the accuracy of determining the pump-probe cross correlation that is used for the convolution.

The fit function to extract the electronic temperature of the metallic state is a Gaussian peak multiplied by a Fermi-Dirac distribution, convolved with a Gaussian peak accounting for the energy resolution of the experiment (50 meV).

References

1. Ahn, C. H., Triscone, J. M. & Mannhart, J. Electric field effect in correlated oxide systems. Nature 424, 1015–1018 (2003).
2. Grotz, B. et al. Charge state manipulation of qubits in diamond. Nat. Commun. 3, (2012).
3. Hwang, H. Y. et al. Emergent phenomena at oxide interfaces. Nat. Mater. 11, 103–113 (2012).
4. Caviglia, A. D. et al. Electric field control of the LaAlO3/SrTiO3 interface ground state. Nature 456, 624–627 (2008).
5. Klingshirn, C., Meyer, B., Waag, A., Hoffmann, A. & Geurts, J. Zinc Oxide - From Fundamental

Properties Towards Novel Applications. Springer Series in Materials Science (2010).

6. Huang, M. H. et al. Room-temperature ultraviolet nanowire nanolasers. Science 292, 1897–1899 (2001).

7. Basov, D. N., Averitt, R. D., Van Der Marel, D., Dressel, M. & Haule, K. Electrodynamics of correlated electron materials. Rev. Mod. Phys. 83, 471–541 (2011).

8. Wen, H. et al. Structural and electronic recovery pathways of a photoexcited ultrathin VO_2 film. Phys. Rev. B 88, (2013).

9. Mott, N. Metal-Insulator Transitions. Taylor&Francis Ltd London (1974).

10. Abrahams, E., Kravchenko, S. V. & Sarachik, M. P. Colloquium: Metallic behavior and related phenomena in two dimensions. Rev. Mod. Phys. 73, 251–266 (2001).

11. McKeown Walker, S. et al. Control of a Two-Dimensional Electron Gas on $SrTiO_3$ (111) by Atomic Oxygen. Phys. Rev. Lett. 113, 1–5 (2014).

12. Rödel, T. C. et al. High-density two-dimensional electron system induced by oxygen vacancies in ZnO. Phys. Rev. Mater. 2, 1–7 (2018).

13. Ozawa, K. & Mase, K. Metallization of ZnO (10-10) by adsorption of hydrogen, methanol, and water: Angle-resolved photoelectron spectroscopy. Phys. Rev. B - Condens. Matter Mater. Phys. 81, 1–6 (2010).

14. Deinert, J.-C., Hofmann, O. T., Meyer, M., Rinke, P. & Stähler, J. Local aspects of hydrogen-induced metallization of the ZnO(10-10) surface. Phys. Rev. B 91, 235313 (2015).

15. Chernikov, A., Ruppert, C., Hill, H. M., Rigosi, A. F. & Heinz, T. F. Population inversion and giant bandgap renormalization in atomically thin WS_2 layers. Nat. Photonics 9, 466–470 (2015).

16. Huber, R. et al. How many-particle interactions develop after ultrafast excitation of an electron-hole plasma. Nature 414, 286–289 (2001).

17. Giannetti, C. et al. Ultrafast optical spectroscopy of strongly correlated materials and high-temperature superconductors: a non-equilibrium approach. Adv. Phys. 65, 58–238 (2016).

18. Huang, L., Callan, J. P., Glezer, E. N. & Mazur, E. GaAs under Intense Ultrafast Excitation : Response of the Dielectric Function. Phys. Rev. Lett. 1, 185–188 (1998).

19. Cavalleri, A. et al. Femtosecond Structural Dynamics in VO_2 during an Ultrafast Solid-Solid Phase Transition. Phys. Rev. Lett. 87, 23 (2001).

20. Wall, S. et al. Ultrafast disordering of vanadium dimers in photoexcited VO_2. Science 362, 572–576 (2018).

21. Morrison, V. R. et al. A photoinduced metal-like phase of monoclinic VO_2 revealed by ultrafast electron diffraction. Science 346, (2014).

22. Wegkamp, D. & Stähler, J. Ultrafast dynamics during the photoinduced phase transition in VO_2. Prog. Surf. Sci. 90, 464–502 (2015).

23. Iwai, S. et al. Ultrafast Optical Switching to a Metallic State by Photoinduced Mott Transition in a Halogen-Bridged Nickel-Chain Compound. Phys. Rev. Lett. 91, 3–6 (2003).

24. Stojchevska, L. et al. Ultrafast Switching to a Stable Hidden Quantum State in an Electronic Crystal. Science 344, 177–180 (2014).

25. Yu, G., Lee, C. H., Heeger, A. J., Herron, N. & McCarron, E. M. Transient photoinduced

conductivity in single crystals of $YBa_2Cu_3O_{6.3}$: Photodoping to the metallic state. Phys. Rev. Lett. 67, 2581–2584 (1991).

26. Zhang, Y. Electronic structures of impurities and point defects in semiconductors. Chinese Phys. B 27, (2018).

27. Katsumoto, S., Komori, F., Sano, N. & Kobayashi, S. Fine Tuning of Metal-Insulator Transition in $Al_{0.3}Ga_{0.7}As$ Using Persistent Photoconductivity. J. Phys. Soc. Jpn. 56, 2259 (1987).

28. Lany, S. & Zunger, A. Anion vacancies as a source of persistent photoconductivity in II-VI and chalcopyrite semiconductors. Phys Rev B 72, 035215 (2005)

29. Foglia, L. et al. Revealing the competing contributions of charge carriers , excitons , and defects to the non-equilibrium optical properties of ZnO. Struct. Dyn. 6, 034501 (2019).

30. Janotti, A. & Van De Walle, C. G. Fundamentals of zinc oxide as a semiconductor. Reports Prog. Phys. 72, (2009).

31. Lisowski, M. et al. Ultra-fast dynamics of electron thermalization, cooling and transport effects in Ru(001). Appl. Phys. A 78, 165–176 (2004).

32. Bovensiepen, U., Gahl, C. & Wolf, M. Solvation Dynamics and Evolution of the Spatial Extent of Photoinjected Electrons in D_2O/Cu(111). J. Phys. Chem. B 107, 8706–8715 (2003).

33. King, S. B., Broch, K., Demling, A. & Stähler, J. Multistep and multiscale electron transfer and localization dynamics at a model electrolyte/metal interface. J. Chem. Phys. 150, 041702 (2019).

34. Cui, X. et al. Transient excitons at metal surfaces. Nat. Phys. 10, 505–509 (2014).

35. Hendry, E., Koeberg, M. & Bonn, M. Exciton and electron-hole plasma formation dynamics in ZnO. Phys. Rev. B 76, 045214 (2007).

36. Versteegh, M. A. M., Kuis, T., Stoof, H. T. C. & Dijkhuis, J. I. Ultrafast screening and carrier dynamics in ZnO: Theory and experiment. Phys. Rev. B 84, 1–19 (2011).

37. Deinert, J.-C. et al. Ultrafast Exciton Formation at the ZnO (10-10) Surface. Phys. Rev. Lett. 113, 1–5 (2014).

38. Liu, F., Ziffer, M. E., Hansen, K. R., Wang, J. & Zhu, X. Direct Determination of Band-Gap Renormalization in the Photoexcited Monolayer MoS_2. Phys. Rev. Lett. 122, 246803 (2019).

39. Yang, S. L., Sobota, J. A., Kirchmann, P. S. & Shen, Z. X. Electron propagation from a photo-excited surface: Implications for time-resolved photoemission. Appl. Phys. A 116, 85–90 (2014).

40. Kronik, L. & Shapira, Y. Surface photovoltage phenomena: theory, experiments and applications. Surf. Sci. Rep. 37, 1–206 (1999).

41. Rettig, L., Kirchmann, P. S. & Bovensiepen, U. Ultrafast dynamics of occupied quantum well states in Pb/Si(111). New J. Phys. 14, (2012).

42. Göpel, W. & Lampe, U. Influence of defects on the electronic structure of zinc oxide surfaces. Phys. Rev. B 22, 12 (1980).

43. Penfold, T. J. et al. Revealing hole trapping in zinc oxide nanoparticles by time-resolved X-ray spectroscopy. Nat. Commun. 9, 1–9 (2018).

44. Sezen, H. et al. Evidence for photogenerated intermediate hole polarons in ZnO. Nat. Commun. 6, 6901 (2015).

Acknowledgements Funded by the Deutsche Forschungsgemeinschaft (DFG) – Projektnummer 182087777 – SFB 951.

Author contributions L.G. and S.V. did the experiments, L.G. analyzed the data. L.G. and J.S. wrote the manuscript. J.S. guided the work. All authors contributed to discussions.

Data availability The datasets analysed during the current study are available from the corresponding author on reasonable request.

Additional information Supplementary material is available for this paper. Correspondence and requests for materials should be addressed to L.G. (e-mail: gierster@fhi-berlin.mpg.de).

Competing financial interests The authors declare no competing interests.

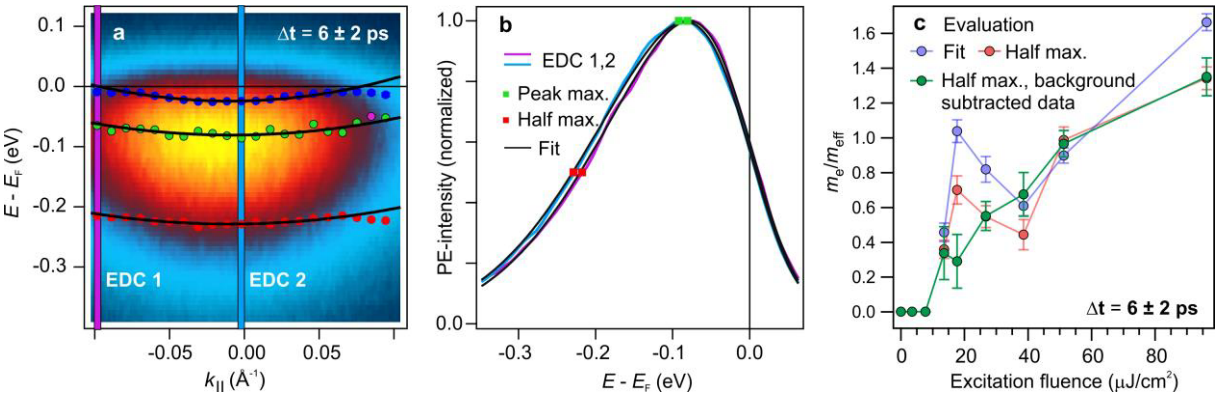

Extended Data Figure 1 Different evaluations of the angular distribution of the photoresponse. a, Angular distribution at a delay of 6 ± 2 ps after resonant photoexcitation with a fluence of 27 μJ/cm^2. Blue: Peak positions from fitting energy distribution curves at different k_{II} (e.g. EDC 1, EDC 2 as indicated with the blue/purple boxes) with a Gaussian peak multiplied by a Fermi-Dirac distribution and convolved with another Gaussian peak to account for the energy resolution (50 meV). Fits to the exemplary spectra are shown in b. Green: Peak maximum of the EDC, red: position of the low energy edge half maximum, numerically determined, as shown in b. The black lines in a are fits with $E(k_{II})=E_0 + \hbar^2k_{II}^2/(2m_{eff})$; m_{eff} = 1.2(1) m_e (blue), m_{eff} = 1.7(5) m_e (green) and m_{eff} = 1.8(3) m_e (red). c, Comparison of the curvature for different fluences; error bars represent standard deviations. Blue: Evaluation from fitting. Green and red: evaluation by determining the half maximum numerically. For the green data points the background at negative delays was subtracted. For low fluences smaller than the PIPT threshold, the background has to be subtracted in order to identify the (localized) character of the excitation, because the photoinduced change is small. Clearly, independent of the evaluation method, we find a free-electron-like band with positive curvature and that the curvature increases as a function of photodoping.

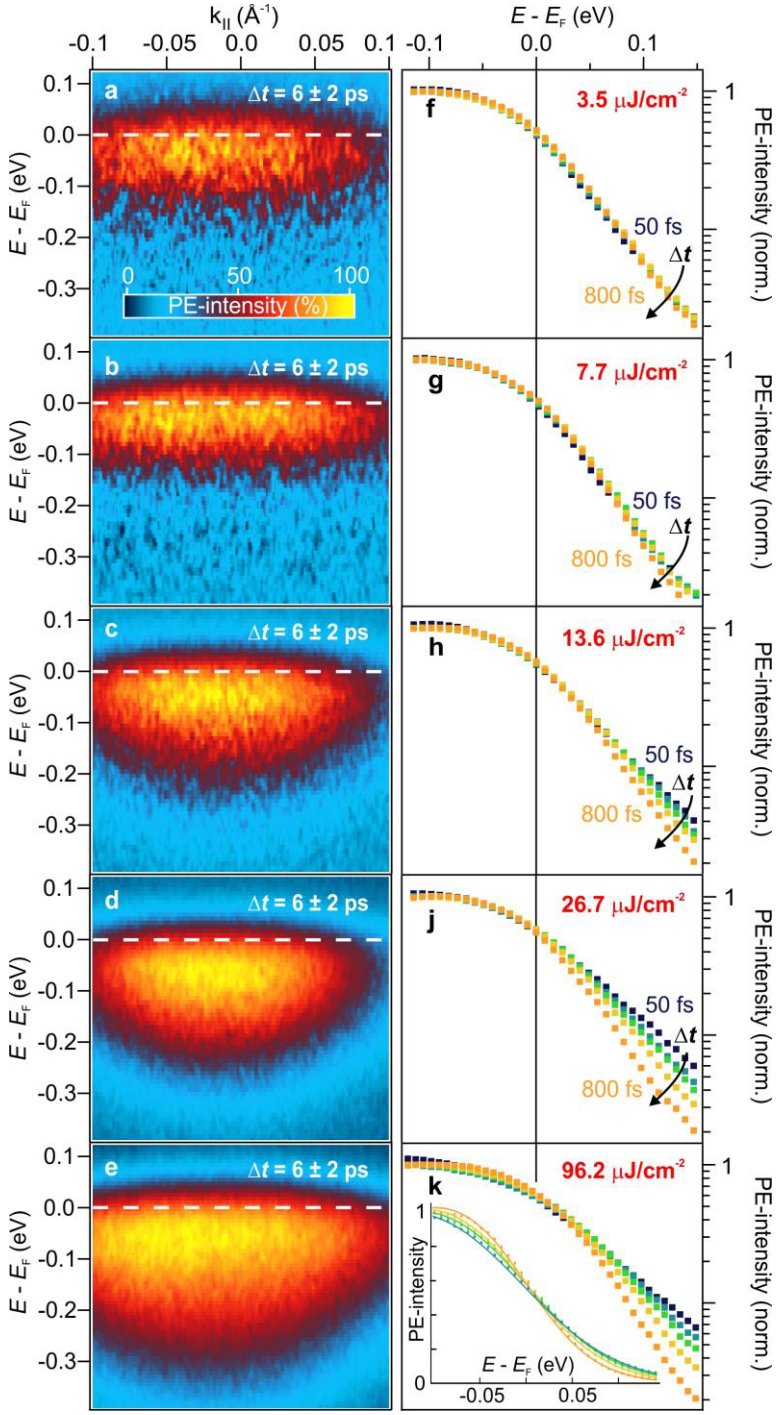

Extended Data Figure 2 Fluence dependence of the photoinduced response. a-e, Angular distribution of the photoinduced change at 6±2 ps below and above the PIPT threshold F_C (13.6 μJ/cm²). Below F_C , the pump induces a non-dispersive state below E_F. Above F_C , a dispersive band evolves, with increasing bandwidth and curvature. For all fluences, the band is cut by the equilibrium Fermi level. f-k, Corresponding angle-integrated PE-spectra (log. scale, normalized) for different pump-probe delays (50 fs to 800 fs). Below F_C, all spectra are identical. Above F_C the high energy tail shows hot electron gas cooling as characteristic for photoexcited metals. The delay dependence is described by Fermi-Dirac distributions with varying temperatures (see non-log. scale data with Fermi-Dirac distribution fits in the inset in k).

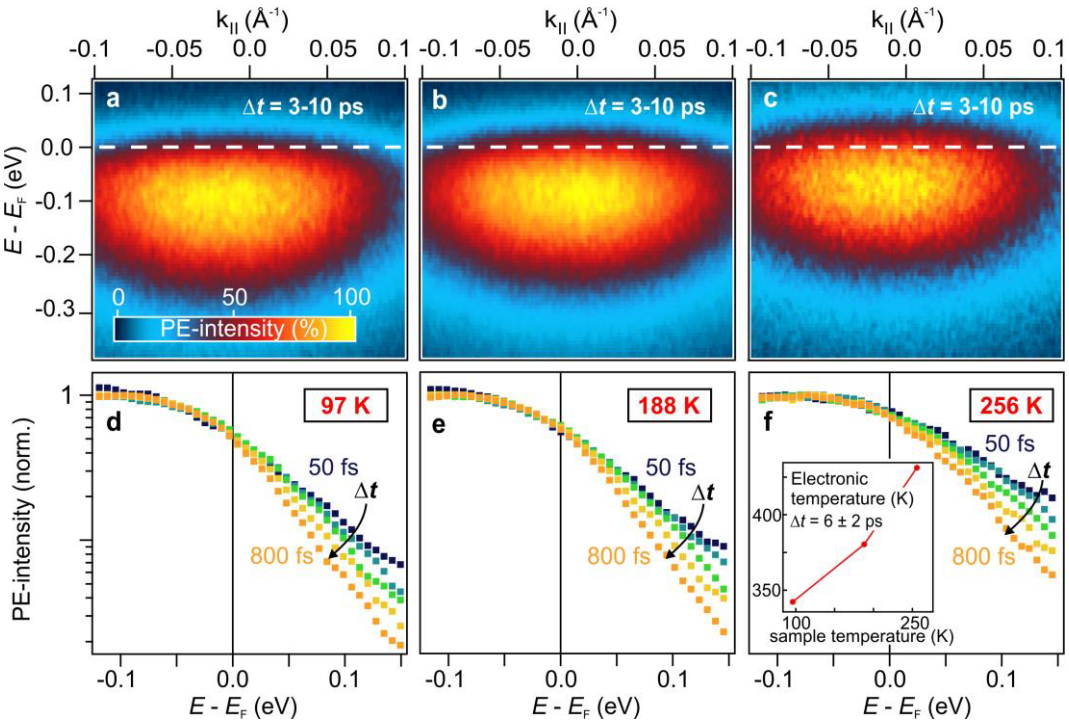

Extended Data Figure 3 Temperature dependence of the photoresponse. a-c, Angle-resolved PE spectra at 97, 188 and 256 K, respectively, averaged across pump-probe delays between 3 and 10 ps. All show a free electron-like band. d-f, Corresponding angle-integrated spectra showing the hot electron gas cooling within the first ps, characteristic for the surface metal phase. The inset of f shows that, after equilibration with the lattice at a late delay of 6 ± 2 ps, the electron (lattice) temperature also increases with the sample temperature (analysis as described in Methods). This shows that the photoinduced SMT works at least up to 256 K.